Two-photon planar laser-induced fluorescence of near-wall CO during the interaction between a flame and a cooling air film

Antoine Blaise[1], Gilles Godard[1], Alexis Vandel[1], Frédéric Grisch[1], Pradip Xavier[1,*]

1: INSA Rouen Normandie, Univ Rouen Normandie, CNRS, Normandie Univ, CORIA UMR 6614, F-76000 Rouen, France
*Corresponding author: pradip.xavier@coria.fr

Keywords: Combustion, Flame-wall interaction, pollutant emissions, CO-PLIF, OH-PLIF.

ABSTRACT

Reducing the anthropogenic pollutant emissions is a major concern in the aeronautical community. Implementing high-power density core engines made of lighter materials would undoubtedly increase the thermal efficiency and reduce CO_2 emissions. Nevertheless, near-wall combustion processes will become significant, raising concerns regarding thermal management. As a result, walls in aero-engine combustors are commonly cooled, but it also introduces more complex physical phenomena associated to pollutant formation during flame-cooling air interaction (FCAI). This experimental study aims at elucidating the role of the cooling air film on CO emissions during FCAI. The experiments are conducted in an atmospheric pressure and optically-accessible lab-scale combustion test rig dedicated to near-wall combustion. It generates a lean premixed turbulent methane/air V-shaped flame, with one branch of the flame that interacts with an oil-cooled stainless-steel wall. A splash-cooling plate system enables to generate a momentum-controlled parietal cooling air film. The novelty of this study is to develop and implement planar laser-induced fluorescence of the CO molecule (CO-PLIF), complemented by planar laser-induced fluorescence of the OH radical (OH-PLIF) as well as global CO emissions in the exhaust gases. Results show that the excitation of the Hopfield-Birge system enables to detect the Ångström bands and the third positive system. However, significant interferences with C_2 and CN emissions are highlighted, being more pronounced in rich combustion conditions, and originating from the incomplete fuel oxidation as well as the high energy density of the two-photon excitation process. A broadband collection strategy of the Ångström bands is selected, since these interferences are limited in lean combustion regimes. The analysis of the flame dynamics indicates that the increase of the cooling air film momentum shifts the reactive flow away from the wall, but also controls the flame wrinkling through modified aerodynamics. As a result, the flame is not influenced anymore by thermal quenching processes, and can effectively burn further away from the wall. Global emission measurements indicate an increase in CO when the cooling air film momentum increases. While thermal quenching favors a faster oxidation downstream of the flame, the establishment of the cooling air film leads to a longer flame with more production areas. CO-PLIF imaging concurs this phenomenon, with a CO distribution all along the wall when the cooling air film is well established.

1. Introduction

Reducing the anthropogenic pollutant emissions is of major concern in the aeronautical community. The aviation sector produces 3% of the global carbon dioxide (CO_2) emissions, with an associated radiative forcing more than 1.5 W.m^{-1}. With an indirect radiative forcing of 0.2 W.m^{-1}, CO plays a major role in the atmospheric chemistry leading to ozone (O_3) formation and presents direct harmful health effects. Because the international authorities (ICAO, ATAG, IEA) forecast an increase in the air traffic between 2% to 4% per year until 2050, it is therefore mandatory to further consider technological breakthroughs in order to shrink CO emissions in future aircraft engines.Though hydrogen combustion and electrification are two avenues of research towards a complete decarbonization of the aviation, they still remain at a development stage and require significant modifications in architecture of the propulsion systems. In a short term, sustainable aviation fuels (SAF) represent a promising candidate to quickly move towards global aircraft pollutant emission reduction: according to the Airport Cooperative Research Program, a blend of 50% SAF is expected to lead to a reduction of carbon monoxide by nearly 11%. Thus, a constant effort to optimize current combustion technologies, especially regarding pollutant emissions is required.

Near-wall combustion has been studied in the combustion community for decades (Poinsot et al., 2011; Dreizler & Böhm, 2015). Originating from the mutual interactions between the wall, the flow and the flame, it creates huge deviations compared to an unbounded reactive flow. Indeed, the large difference in temperature between the combustor walls (~ 1000 K) and the reactive flow (~ 2500 K) induces heat transfer in the order of MW/m^2, leading to a flame quenching event (Sotton et al., 2005). These enthalpy losses modifiy the thermochemical state of the fluid (Mann et al., 2014; Jainski et al., 2017), the flame structure and its dynamics through strain and curvature (Bruneaux et al., 1996; Foucher et al., 2003; Kaddar et al., 2023), and the wall-bounded flow field (Alshaalan & Rutland, 2002; Gruber et al., 2010). These findings are valid in academic configurations, and do not consider realistic configurations in engines, where thermal management is crucial (Lefebvre & Ballal, 2010). Effusion cooling is one of the most widespread method, which consists in creating a thin cooling air-film which is produced by the coalescence of thousands of small air jets (Kumar et al., 2020; Mendez & Nicoud, 2008). Being at the frontier between aerodynamics, mixing, and wall thermal management, this configuration has been studied with different levels of complexity (Behrendt et al., 2008), but the addition of combustion with the presence of an active flame front has been reported very recently, even if scarse studies are reported in the literature (Feist et al., 2003; Lange et al., 2012).

The physics of flame-cooling air interaction (FCAI) has been investigated, both experimentally and numerically. Built on the findings of classical flame-wall interaction processes, Rivera et al. (2019) conducted global measurements consisting in flame visualization and CO measurements in the

exhaust with the presence of single wall coolant jet, highlighting a reduction in CO emissions due to a better oxygenation. The same configuration was numerically investigated and showed the importance of the blowing ratio parameter on the flame dynamics, while mixing reduced CO mass fractions (Palulli et al., 2021). Another configuration was studied with a realistic injector producing a swirled flow field and an effusion plate (Hermann et al., 2019). Results indicated a strong near-wall activity between the cooling air film and the reactive flow (Greifenstein et al., 2019). Detailed examination of mixing showed that the latter can retro-act on the incoming premixed gases, modifying the chemical conditions of CO production (Greifenstein & Dreizler, 2021b). In contrast, near the cooling air film, chemical quenching was observed with a modification of the CO oxidation mechanism (Greifenstein & Dreizler, 2021a). These conclusions were recently extended by identifying different mechanisms that affect the CO chemistry during its production, oxidation, and exhaust phases (Greifenstein & Dreizler, 2023).

Carbon monoxide (CO) can be optically probed through laser-induced fluorescence. Various studies are reported in the literature, including flame-wall interaction (FWI) configurations (Jainski et al., 2017; Greifenstein & Dreizler, 2021a). Nevertheless, they are restricted to pointwise measurements with a statistical analysis. The study of Voigt et al. (2017) provides a demonstration of planar two-photon laser-induced fluorescence of CO (CO-PLIF) with an application to effusion walls. In this article, the authors propose to implement the CO-PLIF laser-based diagnostic on a realistic yet academic case retrieved mimicking the flame-cooling air interaction (FCAI), and to investigate systematically the influence of the cooling air film on the near-wall CO formation mechanisms.

2. Experimental methods

2.1. Calibration flat burner

In order determine the excitation and collection strategies for the CO-PLIF, but also to analyze the CO signals in reactive conditions, a calibration flat burner with internal cooling is implemented. This burner is a good candidate for this task since it can produce a laminar premixed flame with a flow field, a gas composition, and a temperature profile that can be easily measured and numerically modelled. The burner is made of a cylindrical bronze porous plate with a diameter of 20 mm, inserted into a stainless-steel shroud ring. The burner has a water inlet and outlet, as well as a gas inlet. In this study, a laminar premixed methane/air flat flame is generated with a given equivalence ratio, ϕ, through separate thermal mass flow controllers: methane is controlled by a Bronkhorst EL-FLOW flowmeter with a range of 0.01 g.s^{-1}, while synthetic air (Linde, instrument 5) is controlled by an EL-FLOW Bronkhorst flowmeter with a range of 8 L.min^{-1}. Mixing of the two flow streams is performed 3 m upstream of the burner. The small fuel and oxidizer flow rates allow to obtain a flame that is located in the vicinity of the porous plate. The internal cooling enables to

adjust the porous temperature. This boundary condition creates enthalpy losses between the flame and the wall, acting as a flame stabilization method. The temperature profile above the burner is therefore controlled by the equivalence ratio, but also by the heat losses to the porous plate. The numerical twin of this setup is performed with the one-dimensional burner stabilized flame model given by the Cantera library, combined with the Gri-Mech 3.0 chemical scheme (Goodwin et al., 2021). An example of the flame is provided in Fig. 1, where the reference axis refers to the porous plate. The CO concentration (black curve) depicts the typical production and oxidations branches, which both depend on temperature.

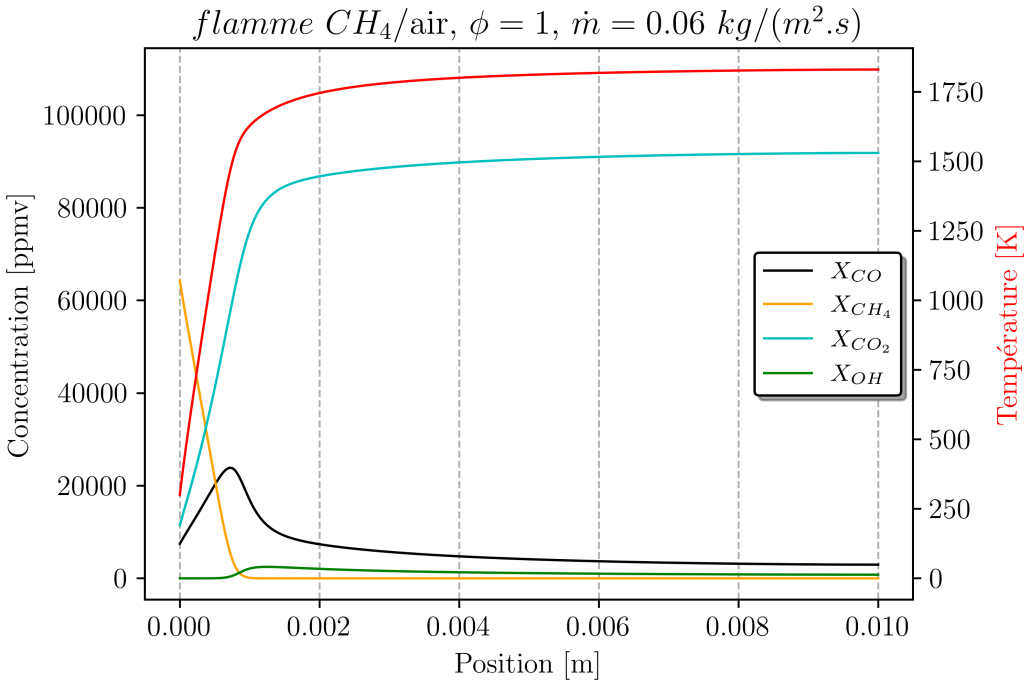

Figure 1. Profiles of temperature and species in a one-dimensional burner stabilized flame model of a premixed stoechiometric methane/air flame.

2.2. CENTOR combustion test rig

Flame-cooling air interaction is generated on an academic test bench, CENTOR (*combustion test bench to observe near-wall energy processes*) from CORIA laboratory, that generates a perfectly premixed V-shaped methane/air flame in an optically accessible environment (Petit et al., 2023). Gaseous methane and air are injected in a plenum at the inlet of the test rig. Gas flow rates are controlled by using mass flow controllers: air flow rate is controlled by a Bronkhorst In Flow F206-AI while Bronkhorst El Flow F203-AV is used to control methane flow. Temperature of the gas flows are set via two 4 kW air heaters (Tutco SureHeat). The two streams are directed into a plenum, where they are mixed and homogenized through a porous media plate, a layer of glass beads, a perforated plate and a honeycomb layer successively. At the exit of the last mixing stage, the flow

is directed to a convergent nozzle to obtain a uniform flat laminar flow. The turbulence of the premixed flow is generated by a turbulence generator, made of three 80 mm x 80 mm grids (Mazellier et al., 2010; Cardin, 2013). The Reynolds number at the exit of the turbulence generator is $\mathrm{Re} = 15\,500$, based on the hydraulic diameter of the convergent exit. A turbulent V-shaped flame, represented in blue in Figure 3, is anchored on a 5mm-diameter ceramic rod. The rod is located 20 mm upstream and 20 mm away from the wall of interest, allowing an optically accessible interaction between one branch of the V-shaped flame and a stainless-steel wall. The wall is thermally-controlled via a circulator (Julabo H30-M1-CU) operating with a high-temperature thermal oil (Julabo H350). At the bottom of the wall, a splash cooling device produces an air-film from a plenum (10 x 70 x 2 mm^3). The cooling air flow is deflected on a 0.5 mm thick lip (2.5 mm protrusion in the mainstream passage) and is blown along the wall with a given momentum. Thus, physico-chemical processes occurring during an interaction between a turbulent methane-air flame at atmospheric pressure and a developing parietal air-film can be investigated by specifically varying the flow momentum of the cooling air flow (i.e. blowing ratio, M). In this study, the main flow rate is set to 22 $g.s^{-1}$, with an equivalence ratio, $\phi = 0.90$. The blowing ratios are ranging from M = 0.5 to M = 3.0. The test rig is fully water-cooled, never exceeding 330 K. Three high-purity fused silica windows (200 to $2200\,nm$ transmission range, Corning grade 7980-5F) enable to have two side and frontal views of the reactive flow and the wall of interest. A zenithal window on top of the burner enables the laser sheets to probe perpendicularly the near-wall region of interest. Burnt gases are extracted via an off-axis chimney. More details on the CENTOR test bench can be found in Petit et al. (2023).

2.3. Gas analyzer

To assess CO emissions directly downstream of the interaction plate, a combustion analyzer (ECOM J2KN Pro Easy) is used. The measurement range is 0-4000 ppm with an uncertainty of $5\,\%$ of the measured value. The analyzer has been calibrated in advance using a 1800 ppmv CO - N_2 gaseous mixture (Air Liquide OTO-SL32). The probe is inserted perpendicularly to the wall in order to conduct pointwise measurements, and then to obtain concentration profiles from the wall.

3. Laser diagnostics

3.1. Two-photon laser induced fluorescence of CO (CO-PLIF)

CO molecules are excited via the Hopfield-Birge system $B^1\Sigma^+(\nu' = 0) \leftarrow X^1\Sigma^+(\nu'' = 0)$, at the maximum of the band head, $\approx$230.1 nm. To achieve such UV radiation, a tunable laser (Sirah PrecisionScan) is used with DCM ($C_{19}H_{17}N_3O$) dissolved in dimethylsulfoxyde (DMSO). The dye

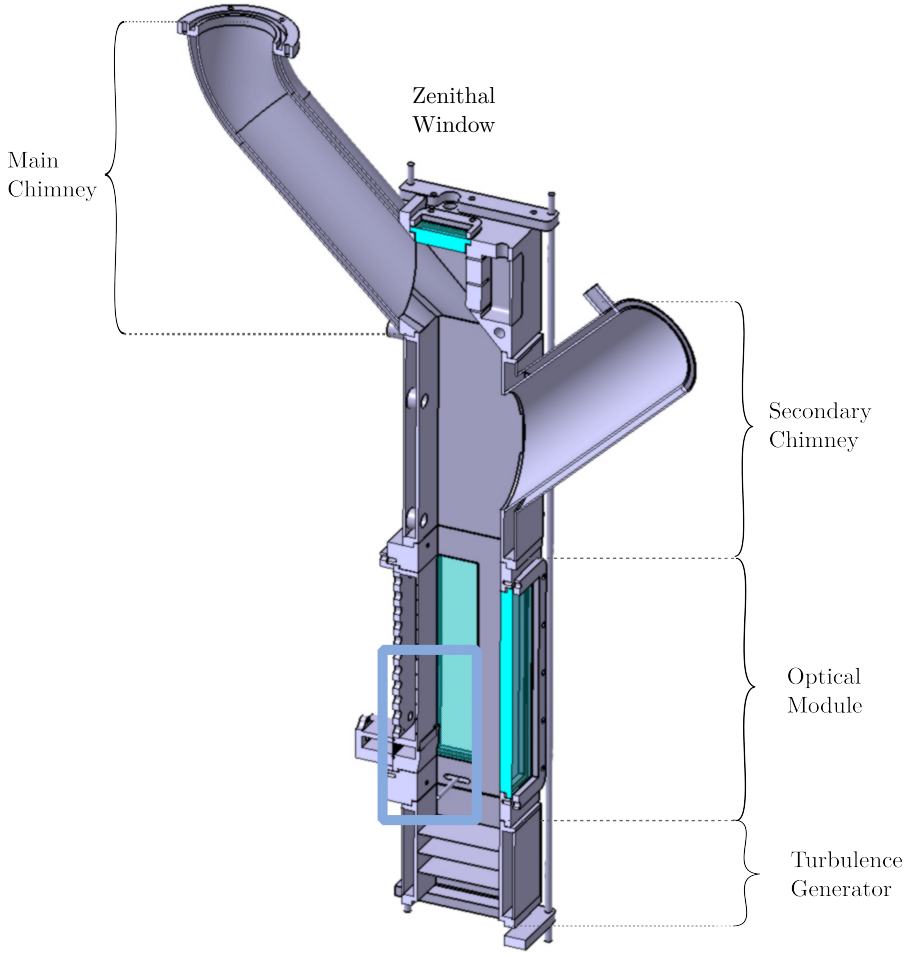

Figure 2. 3D cut-view of the CENTOR test rig.

laser is pumped by a Nd:YAG laser (Quanta Ray, Spectra Physics) operating at 10 Hz, and with an energy of 500 mJ per pulse (at 1064 nm). The frequency-doubled beam (532 nm) is injected into the oscillator, producing a fluorescence seed between 640 and 660 nm. A grating enables to select the subsequent wavelenght of interest (≈654 nm). This fluorescence seed is then amplified through two capillary cavities, to produce a high energy laser beam. The third harmonic of the pump laser (355 nm) is mixed with the amplified fluorescent beam (654 nm) inside a temperature-controlled BBO crystal. The fine displacement of its position allows to obtain the desired wavelength while residuals at other wavelenghts are removed with the use of a single Pellin-Broca prism. The output laser beam has a spectral finesse of 0.08 cm^{-1}, and a mean energy of 16 mJ per pulse, with a standard deviation of 2.9 % (based on 3500 pulses). Its wavelength is monitored with a wavemeter (HighFinesse WS6-600), equipped with a collimator and a multimode OH-doped fiber.

For pointwise measurements, the beam is guided towards measurement volume via a periscope made up of two prisms (Newport 10SR25 and 10SR20). A third prism (Newport 10SR20) directs the beam vertically towards the burner. The laser beam then passes through a spherical converging

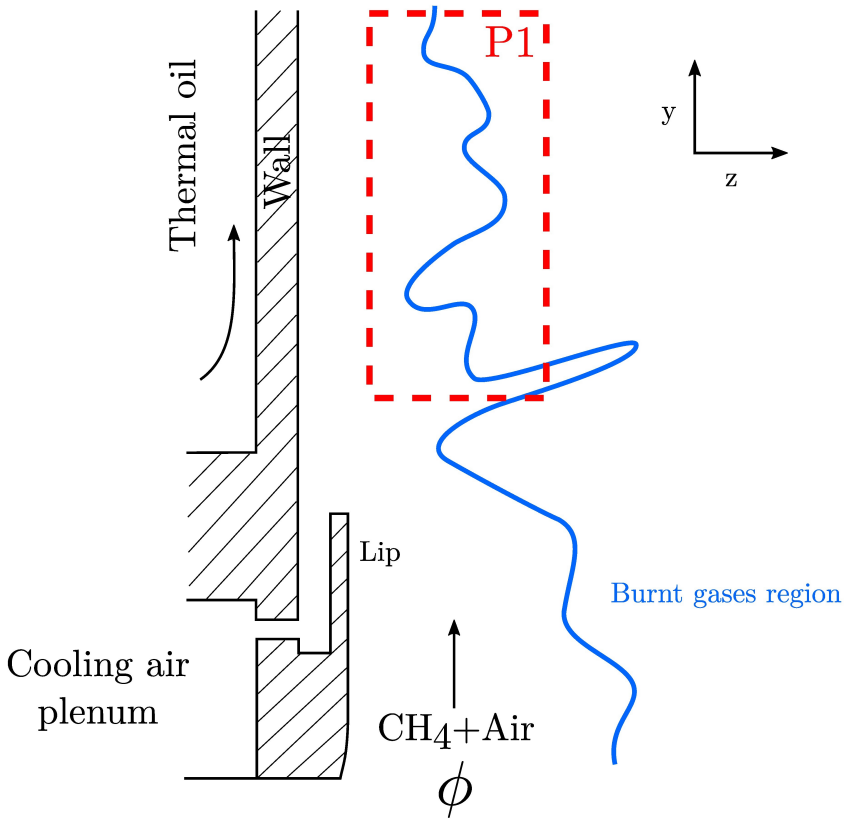

Figure 3. Schematic of the flame-cooling air geometry in the CENTOR burner. The P1 region of interest depicted by the red rectangle refers to the CO-PLIF imaging measurements.

lens with focal length, f=+96 cm, giving an estimated beam waist of 118 μ m in the measurement volume. For two-dimensionnal measurements, a cylindrical divergent UV lens (f=-75 mm) as well as a cylindrical convergent UV lens (f=+125 mm) are added to the aformentionned setup. These two lenses are arranged in a 2f assembly, in order to obtain a collimated laser sheet configuration. Eventually, a convergent cylindrical lens (f=+400 mm) is used to reduce the laser sheet thickness to $\approx$100-150 μ m.

For the spectroscopic analysis, a spectrometer (IsoPlance SCT-320, Roper Scientific) is used. It gathers three gratings, but the one with 300 lines is used in the present study. A biconvex lens (f=+400 mm) is located in front of the spectrometer to focus the imag point of the slit. A high-pass optical filter (LPEF 257 RU, Semrock) is inserted in front of the spectrometer to remove the laser intereferences. An emICCD camera (PIMAX4, Princeton instruments) is connected to the spectrometer to collect the signal. In order to calibrate the spectrometer (wavelength), the Intellical module (Princeton Instrument) made of a Hg/Ne lamp is used. For imaging studies, an emICCD camera (PIMAX4, Princeton instruments) equipped with a f/2.8 100 mm UV Cerco lens is implemented to collect the emitted fluorescence. Two high-pass optical filters (ZULO325 and BEB430, Asahi) are placed in front of the camera to remove the laser interferences as well as other interfer-

ences. It will be shown in the results, that the sole Ångström bands of the $B^1\Sigma^+ \rightarrow A^1\Pi^+$ system are collected with this optical setup. The camera gate is set to 30 ns while the acquisition is delayed by 100 ns compared to the aperture gate of the OH-PLIF (Sec. 3.2).

3.2. Planar laser induced fluorescence of OH (OH-PLIF)

Planar laser-induced fluorescence (PLIF) on the hydroxyl radical (OH) is implemented on the CENTOR test rig to obtain images of the rod-stabilized flame and track the interfaces between fresh and burnt gases. OH molecule is a popular flame front marker (Grisch & Orain, 2009; Yamamoto et al., 2009). Indeed, OH radicals are produced in the flame front and are still present in the burnt gases. This molecule is excited by means of a tunable dye laser (Quantel TDL90) pumped by a frequency-doubled Nd:YAG laser (532 nm) operating at 10 Hz and set to the $Q_1(5)$ ro-vibrational transition at 282.75 nm. The mean laser energy at the output of the dye laser is 20 mJ per pulse. A set of optics is then used to shape the laser beam into a 30-mm high laser sheet. Two cylindrical lenses of focal distances f=-40 mm and f= +300mm respectively are used to generate a collimated laser sheet. Then, similarly to CO-PLIF diagnostics, the laser sheet is thinned down to 100 μ m in the region to probe by use of the same spherical lens of focal distance f =+400 mm. Then, the laser sheet penetrates the burner via the zenithal optical access so that is is injected perpendicular to the wall. The near-wall region is probed by tilting with a slight angle the laser sheet. The emitted fluorescence signal is collected at 3.33 Hz with an ICCD camera (PI-MAX 3, Princeton Instrument), equipped with an f/2.8 105 mm UV Cerco lens. A narrow optical band-pass filter (Asahi Spectra, 310$\pm$5 nm) is placed in front of the collection system to only detect the OH fluorescence signal. The camera exposure time is set to 80 ns. The acquisition starts 5 ns prior to the laser pulse.

4. Results

4.1. Emission spectra

The CO emission spectra are recorded in the calibrated flame methane/air flame. Mesurements are pointwise, with a control volume located 6 mm above the porous. Different equivalence ratios, ϕ, are tested, covering lean and rich combustion regimes. Thus, it is possible to assess the influence of various thermochemical states (i.e. temperature and gas composition) on the fluorescence emission spectra. Note that the spectra are time-averaged (500 instantaneous recordings) and background subtracted in order to remove the natural emission of the flame.

The CO fluorescence spectra are shown in Fig. 4. The emission from the Ångström bands $B^1\Sigma^+(\nu' = 0) \rightarrow A^1\Pi^+(\nu'' = 0-4)$ can be identified, at 451 nm, 483 nm, 520 nm, 561 nm, and 508 nm. Furthermore, Other fluorescence bands are observed at 280 nm, 299 nm, 313 nm, and 330 nm, which correspond to the third positive system $b^3\Sigma \rightarrow a^3\Pi$. The evolution of the latter bands are related

to the equivalence ratio, being quite intense for rich flames, but weaker than the Ångström bands in lean conditions. Remarkably, additional broad emission peaks are noticed, exclusively in rich conditions. These emission peaks are associated to the incomplete combustion process retrived in rich conditions, and the photodissociation process due to the high energy density in the control volume (focused beam) that can produce C and O atoms. Moreover, the production of such atoms can be associated with the photodissociation of N_2, thus creating chemical recombination routes to the formation of C_2 and CN. This is in agreement with the literature, with the identification of the some Swan bands of C_2 at 435 nm, 549 nm, and to a less extent 590 nm.

The overall trend for the CO emission peaks are being reduced with the decrease of the equivalence ratio, being explained by the low CO production and therefore a low presence of this molecule in the burnt gases. As a result, the accuracy of the measurement is poorer, as the signal-to-noise ratio is greatly reduced, particularly in the case $\phi = 0.65$. In contrast, for higher equivalence ratios, i.e. $\phi = 1.4$, important interference with C_2 is present, due to the proximity of the emission bands with the ones of CO. Thus, the optical filtering strategy for imaging application would be delicate in rich conditions, and would deserve a detailed analysis to obtain a compromise between a broadband collection strategy associated to a significant deviation, or a narrow bandpass filtering with a much lower signal-to-noise ratio.

In the present study, the equivalence ratio is $\phi = 0.9$, and the addition of the cooling air film would necessarily reduce it. By observing the spectra in Fig. 4, the interferences with CN or C_2 can be neglected, thus enabling the possibility to implement a broadband collection. However, only the Ångström bands (>430 nm) are collected in order to not collect the remaining CN and C_2 that are still detected between 350 and 450 nm.

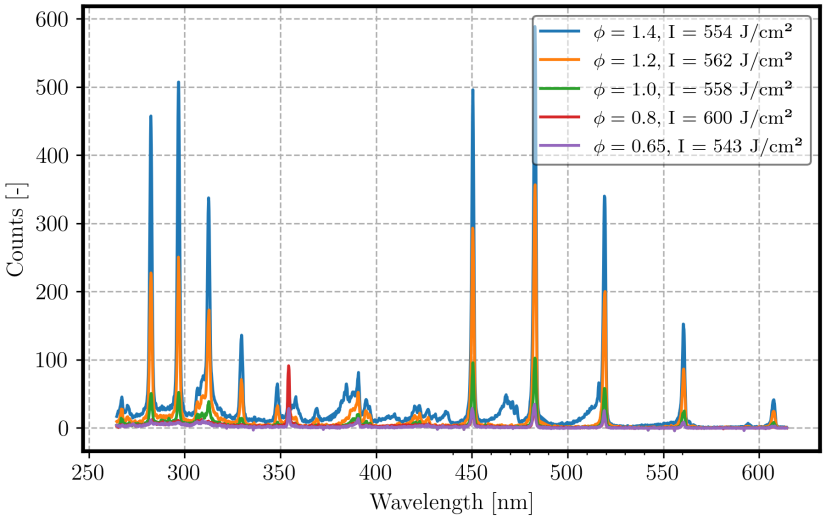

Figure 4. Fluorescence spectra of CO obtained in a methane/air flat flame, for different equivalence ratios, ϕ. The excitation of CO is set to 230.1 nm, while the fluence is adjusted to be roughly identical.

4.2. Flame dynamics

Flame dynamics is firstly assessed, on the academic near-wall combustion rig, CENTOR. The modification of the flame dynamics by increasing the cooling air film at the wall is investigated by observing instantaneous fields of OH (OH-PLIF, Sec. 3.2). Figure 5 shows two instantaneous OH images for two blowing ratios, M = 0.5 (Fig. 5a) and M = 3 (Fig. 5b). The cooling air film flow rate is increased while the mainstream conditions remain identical, with the same equivalence ratio, $\phi = 0.9$.

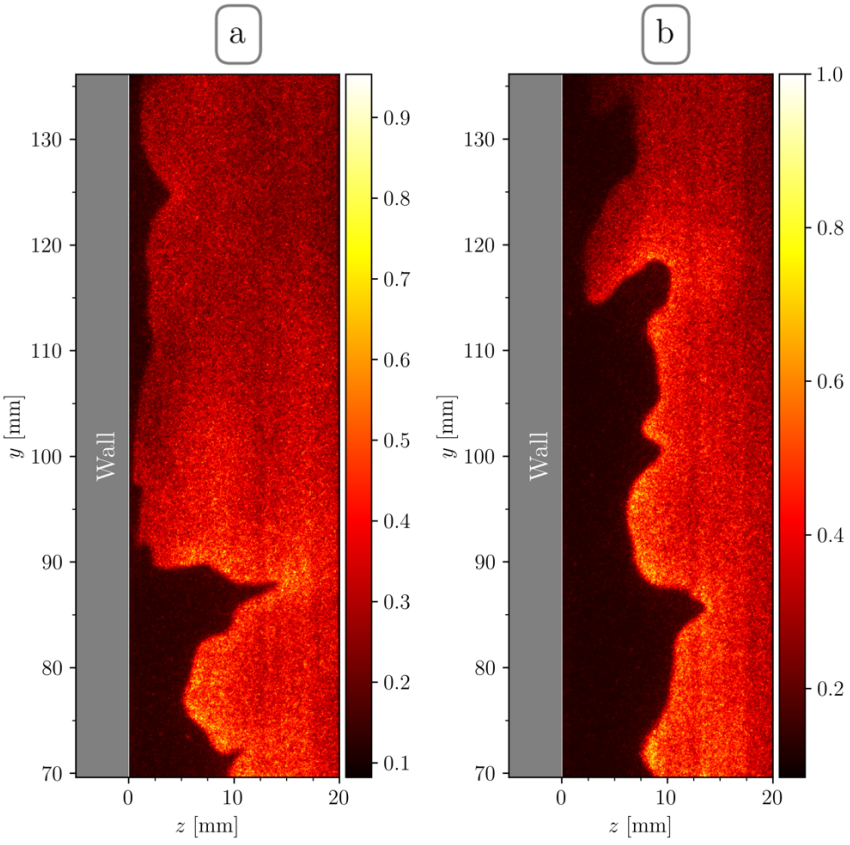

Figure 5. a: OH fluorescence signal for M= 0.5 ; b: OH fluorescence signal for M= 3

The most striking difference between the two conditions is the flame-to-wall distance of the OH interface. When the blowing ratio is small (Fig. 5a), the flame front is very close, and is even thermally quenched at the wall at $y = 90$ mm. The relative intensity of the OH signal agrees with this observation, leading to the establishment of an active flame front upstream and a passive interface downstream. Moreover, the interface wrinkling is larger in the upstream region, being likely driven by the flame dynamics with important levels of curvature, while the interface is smoothened downstream. When the blowing ratio is increased (Fig. 5b), the flame is effectively shifted away from the wall, never touching it in the region of interest. The analysis of the flame wrinkling shows an active flame front that extends more downstream, with associated structures

which are less curved. This could be probably related to the establishment of a shear layer with subsequent turbulent flow structures. In conclusion, the increase of the blowing ratio naturally leads to a better thermal protection of the wall by simply shifting it, but it also impacts on the flame dynamics, with an active flame front which is less affected by the heat losses at the wall.

4.3. Global CO emissions

The analysis of the flame dynamics presented in Sec. 4.2 indicates a dual modification of the flame: a displacement from the wall, being less influenced by the wall heat losses, and an alteration of the flame wrinkling associated to a greater effective burning surface. The analysis of CO emissions by sampling the gas in the exhaust (Sec. 2.3) is reported in Fig. 6. It depicts the mean normalized CO emission profiles along the z axis, i.e. the flame-to-wall distance.

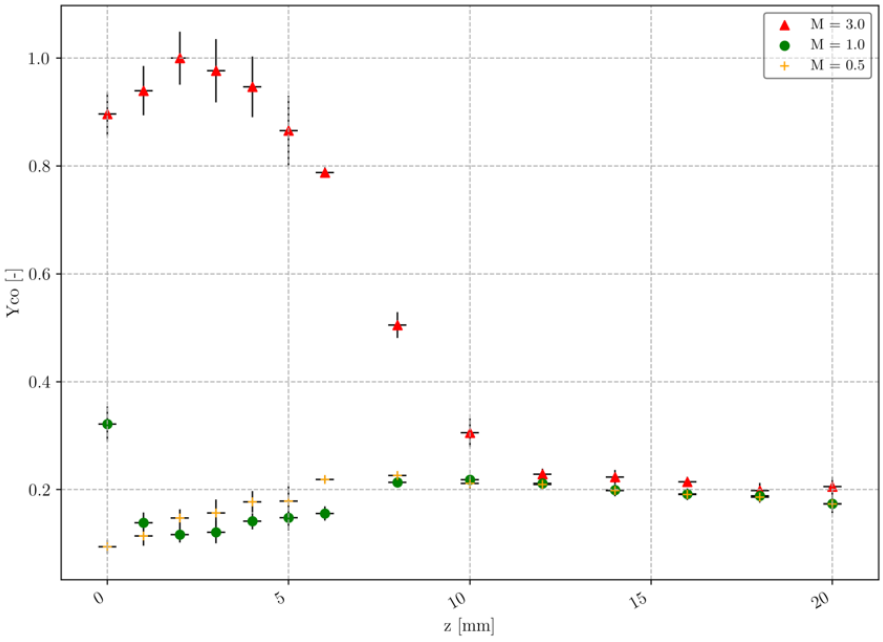

Figure 6. Mean normalized CO concentration profiles for the three blowing ratios, M = 0.5 (cross), M = 1 (circles), and M = 3 (triangles). The wall is located at $z = 0$ mm.

Far away from the wall (z>10 mm), the three profiles all collapse and no differences can be noticed. This is due to the fact that in this region, only burnt gases are retrieved, being away from the flame, where production and oxidation processes occur. Thus, this value is small due to the local conditions which could be close to adiabatic ones. Closer to the wall, three behaviors are observed by varying the blowing ratio. When M = 0.5 (cross), the CO emissions are reduced in the vicinity of the wall (z<5 mm), which could be due to the rapid thermal quenching of the flame so that the CO produced in these regions are then transported in burnt gases where oxidation can take place. when M = 1.0 (circles), this trend is reversed with a peak of CO very close to the wall (z<2 mm).

It is suspected that the longer penetration of the cooling air film will deviate the flame along the burner centerline, and then, creating a longer effective flame surface. When M = 3.0 (triangles), an important increase in CO is observed for z<10 mm. In this case, the flame is shifted from the wall, which is corroborated with the maximum of CO at $z = 2.5$ mm. The large increase of CO emissions is explained as follows. As the cooling air film penetrates more along the wall, it creates an inert layer of air. The reactive flow is then burning away from the wall, with a much longer flame surface. Then, the production rate is increased while the time for oxidation is reduced. Note that this is not in agreement with the literature (Palulli et al., 2021), but it is hypothetised that the generation of the cooling air film must play a primary role since mixing and flame-turbulence interactions are not identical.

4.4. Impact of the flame dynamics on local CO emissions

The analysis of CO emissions in Sec. 2.3 is perfomed in the exhaust gases. Thus it is impossible with this technique to assess the mechanisms of CO formation. To do so, the joint use of OH-PLIF (Sec. 3.2) and CO-PLIF (Sec. 3.1) is conducted in this section, with the aim of validating the collection strategy shown in Sec. 4.1, and the proof-of-concept methodology of conducting CO imaging. Figure 7 presents two pairs of instantaneous images, for M = 0.5 (Fig. 7a) and M = 3.0 (Fig. 7b). The left image of each pair is the field of CO (blue-to-red color scale) while the right one is the field of OH (black-to-red color scale). The wall is located at z =0 mm and the present region of interest refers to the P1 rectangle in Fig. 3.

The OH images are the same as in Fig. 5, but they are cropped in order to match the same imaging area of the CO-PLIF. The CO fields presents a much lower signal-to-noise ratios. Nevertheless, thin layer of higher intensities can be detected. Remarkably, these regions are spatially correlated to the OH interface. It can be concluded that this measured CO is exclusively originating from the flame front (production). It can be noticed that the CO intensities are not constant along the flame front, being related to the local flame structure. A future analysis will be performed to correlate the flame curvature to the intensity of CO. As explained in Secs. 4.3 and 4.2, the flame has an effective flame surface that is larger when the blowing ratio is increased. This is confirmed with the CO images, where the signal stops at $z = 90$ mm for M = 0.5, while it remains till $z = 115$ mm for M = 3.0. Thus the volume-integrated production rate is increased when the blowing ratio is larger, and the flame topology reduces the time for oxidation in the burnt gases. This conclusion is preliminary since it assumes that the flow-turbulence interactions are negligible and that no aerodyanmic/mixing effect take place.

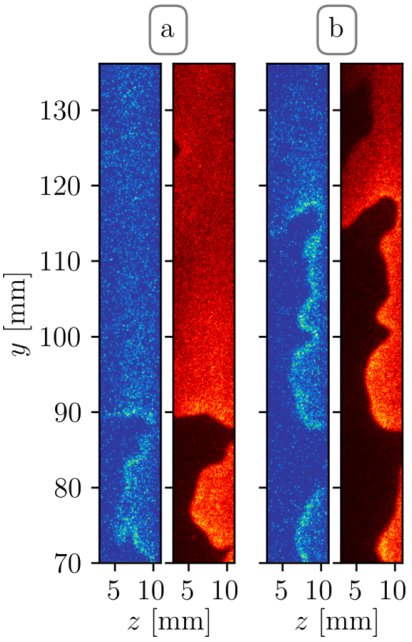

Figure 7. Instantaneous imaging of CO and OH for (a) M = 0.5 and (b) M = 3.0. The left image of each pair corresponds to the CO fluorescence (blue-to-red color scale) and the right image of each pair is the OH fluorescence (black-to-red color scale) The region of interest is shown in Fig. 3 as P1 rectangle.

5. Conclusions

Analysis of carbon monoxide (CO) formation during the interaction of a lean premixed methane/air V-shaped flame and a parietal cooling air film is conducted in the experimental study, by systematically varying the ratio of momentum between the two flows. Planar laser-induced fluorescence of the CO molecule (CO-PLIF), complemented by planar laser-induced fluorescence of the OH radical (OH-PLIF) as well as global CO emissions in the exhaust gases are implemented to assess the relations between the flame dynamics, the global and local CO emissions. The CO fluorescence spectra enable to select a broadband collection strategy, even if some interferences due to C_2 and CN are observed. The increase of the cooling air film momentum results in a modification of the flame topology, being shifted from the wall, with associated larger global CO emissions. These observations are related to a longer CO distribution along the wall, indicating that the cooling air film enables the flame to be not influenced by wall heat losses and to effectively burn further away from the wall, thereby increasing the CO production zones.

Acknowledgements

Financial support was partly provided by the project WALL-EE of the French National Research Agency (ANR), grant no. ANR-19-CE05-0007, as well as the French ministry of higher-education

and research.

References

Alshaalan, T., & Rutland, C. J. (2002). Wall heat flux in turbulent premixed reacting flow. *Combust. Sci. Technol.*, *174*(1), 135–165.

Behrendt, T., Lengyel, T., Hassa, C., & Gerendàs, . M. (2008, 06). Characterization of advanced combustor cooling concepts under realistic operating conditions. In *Turbo expo: Power for land, sea, and air* (Vols. Volume 4: Heat Transfer, Parts A and B, pp. 1801–1814).

Bruneaux, G., Poinsot, K. A. T., & Ferziger, J. H. (1996). Flame-wall interaction simulation in a turbulent channel flow. *Combust. Flame*, *107*(1-2), 27–44.

Cardin, C. (2013). Experimental analysis of laser-induced spark ignition of lean turbulent premixed flames. *Comptes Rendus Mécanique*, *341*(1), 191-200. (Combustion, spray and flow dynamics for aerospace propulsion)

Dreizler, A., & Böhm, B. (2015). Advanced laser diagnostics for an improved understanding of premixed flame-wall interactions. *Proceedings of the Combustion Institute*, *35*(1), 37–64.

Feist, J. P., Heyes, A. L., & Seefelt, S. (2003). Thermographic phosphor thermometry for film cooling studies in gas turbine combustors. *Proceedings of the Institution of Mechanical Engineers, Part A: Journal of Power and Energy*, *217*(2), 193–200.

Foucher, F., Burnel, S., Mounaïm-Rousselle, C., Boukhalfa, M., Renou, B., & Trinite, M. (2003). Flame wall interaction: effect of stretch. *Exp. Therm. Fluid Sci.*, *27*(4), 431–437.

Goodwin, D. G., Speth, R. L., Moffat, H. K., & Weber, B. W. (2021). *Cantera: An object-oriented software toolkit for chemical kinetics, thermodynamics, and transport processes.* `https://www.cantera.org`. (Version 2.5.1)

Greifenstein, M., & Dreizler, A. (2021a). Influence of effusion cooling air on the thermochemical state of combustion in a pressurized model single sector gas turbine combustor. *Combustion and Flame*, *226*, 455–466. doi: https://doi.org/10.1016/j.combustflame.2020.12.031

Greifenstein, M., & Dreizler, A. (2021b). Investigation of mixing processes of effusion cooling air and main flow in a single sector model gas turbine combustor at elevated pressure. *International Journal of Heat and Fluid Flow*, *88*, 108768.

Greifenstein, M., & Dreizler, A. (2023). Influence of effusion cooling air on the co production in the primary zone of a pressurized single sector model gas turbine combustor. *Combustion and Flame*, *248*, 112511.

Greifenstein, M., Hermann, J., Boehm, B., & Dreizler, A. (2019). Flame–cooling air interaction in an effusion-cooled model gas turbine combustor at elevated pressure. *Experiments in Fluids*, *60*(1), 10.

Grisch, F., & Orain, M. (2009, 12). Role of planar laser-induced fluorescence in combustion research. *Aerosp. Lab.*.

Gruber, A., Sankaran, R., & E. R. Hawkes, J. H. C. (2010). Turbulent flame–wall interaction: a direct numerical simulation study. *J. Fluid Mech.*, *658*, 5–32.

Hermann, J., Greifenstein, M., Boehm, B., & Dreizler, A. (2019). Experimental investigation of global combustion characteristics in an effusion cooled single sector model gas turbine combustor. *Flow, Turbulence and Combustion*, *102*(4), 1025–1052.

Jainski, C., Rißmann, M., Böhm, B., Janicka, J., & Dreizler, A. (2017). Sidewall quenching of atmospheric laminar premixed flames studied by laser-based diagnostics. *Combust. Flame*, *183*, 271–282.

Kaddar, D., Steinhausen, M., Zirwes, T., Bockhorn, H., Hasse, C., & Ferraro, F. (2023). Combined effects of heat loss and curvature on turbulent flame-wall interaction in a premixed dimethyl ether/air flame. *Proceedings of the Combustion Institute*, *39*, 2199–2208.

Kumar, K. R. Y., Qayoum, A., Saleem, S., & Qayoum, F. (2020, apr). Effusion cooling in gas turbine combustion chambers - a comprehensive review. *IOP Conference Series: Materials Science and Engineering*, *804*(1), 012003.

Lange, L., Heinze, J., Schroll, M., Willert, C., & Behrendt, T. (2012). Combination of planar laser optical measurement techniques for the investigation of pre-mixed lean combustion, 16th int. In *Symposium on applications of laser techniques to fluid mechanics, lisbon, portugal.*

Lefebvre, A. H., & Ballal, D. R. (2010). *Gas turbine combustion: alternative fuels and emissions*. CRC press.

Mann, M., Jainski, C., Euler, M., Böhm, B., & Dreizler, A. (2014). Transient flame–wall interactions: Experimental analysis using spectroscopic temperature and co concentration measurements. *Combust. Flame*, *161*(9), 2371–2386.

Mazellier, N., Danaila, L., & Renou, B. (2010). Multi-scale energy injection: a new tool to generate intense homogeneous and isotropic turbulence for premixed combustion. *Journal of Turbulence*, *11*, N43.

Mendez, S., & Nicoud, F. (2008). Large-eddy simulation of a bi-periodic turbulent flow with effusion. *Journal of Fluid Mechanics*, *598*, 27–65.

Palulli, R., Talei, M., & Gordon, R. L. (2021). Analysis of near-wall CO due to unsteady flame–cooling air interaction. *Flow Turb. Combust.*, *107*, 343–365.

Petit, S., Quevreux, B., Morin, M., Guillot, R., Grisch, F., & Xavier, P. (2023). Experimental investigation of flame-film cooling interactions with an academic test rig and optical laser diagnostics. *ASME J. Turbomach.*, *145*(4), 041007.

Poinsot, T., Garcia, M., Senoner, J. M., Gicquel, L., & Vermorel, O. (2011). Numerical and physical instabilities in massively parallel les of reacting flows. *Journal of Scientific Computing*, *49*, 78–93.

Rivera, J. E., Gordon, R. L., Brouzet, D., & Talei, M. (2019). Exhaust CO emissions of a laminar premixed propane–air flame interacting with cold gas jets. *Combust. Flame*, *210*, 374–388.

Sotton, J., Boust, B., Labuda, S. A., & Bellenoue, M. (2005). Head-on quenching of transient laminar flame: Heat flux and quenching distance measurements. *Combustion Science and Technology*, *177*(7), 1305–1322.

Voigt, L., Heinze, J., Aumeier, T., Behrendt, T., & di Mare, F. (2017). Quantitative co plif measurements in aeroengine gas turbine combustion chambers under realistic conditions. In *Turbo expo: Power for land, sea, and air* (Vol. 50916, p. V006T05A004).

Yamamoto, K., Ozeki, M., Hayashi, N., & Yamashita, H. (2009). Burning velocity and oh concentration in premixed combustion. *Proc. Combust. Inst.*, *32*(1), 1227–1235.